

This discussion paper is/has been under review for the journal Atmospheric Chemistry and Physics (ACP). Please refer to the corresponding final paper in ACP if available.

A new scheme for sulphur dioxide retrieval from IASI measurements: application to the Eyjafjallajökull eruption of April and May 2010

E. Carboni¹, R. Grainger¹, J. Walker¹, A. Dudhia¹, and R. Siddans²

¹AOPP, Physic department, University of Oxford, Oxford, UK

²Rutherford Appleton Laboratory, Didcot, UK

Received: 17 April 2012 – Accepted: 26 April 2012 – Published: 8 May 2012

Correspondence to: E. Carboni (elisa@atm.ox.ac.uk)

Published by Copernicus Publications on behalf of the European Geosciences Union.

Title Page

Abstract

Introduction

Conclusions

References

Tables

Figures

◀

▶

◀

▶

Back

Close

Full Screen / Esc

Printer-friendly Version

Interactive Discussion



Abstract

A new algorithm for the retrieval of sulphur dioxide (SO_2) from IASI data has been developed based on optimal estimation theory. It uses the IASI channels between 1000–1200 and 1300–1410 cm^{-1} . These regions include the two SO_2 absorption bands (the ν_1 and ν_3 bands) centred at about 7.3 and 8.7 microns, respectively. The retrieval assumes a Gaussian distribution for the vertical SO_2 profile and returns the SO_2 column amount in Dobson units (DU) and the altitude of the plume in millibar (mb). Radiative transfer computations that generate the forward modelled spectra (against which the measurements are compared) are based on RTTOV and ECMWF meteorological data. The retrieval includes a comprehensive error budget for every pixel. This is derived from an error covariance matrix that is based on the SO_2 -free climatology of the differences between the IASI and forward modelled spectra. The IASI forward model includes the ability to simulate a cloud or ash layer in the atmosphere. This feature is used to illustrate that: (1) the SO_2 retrieval is not affected by underlying cloud but is affected if the SO_2 is within or below a cloud layer; (2) it is possible to discern if ash (or other atmospheric constituents not considered in the error covariance matrix) affects the retrieval using quality control based on the fit of the measured spectrum by the forward modelled spectrum. In this work the algorithm is applied to follow the behaviour of SO_2 plumes in atmosphere for the Eyjafjallajökull eruption during April and May 2010 in terms of SO_2 amount. From 14 April to 4 May (during phase I and II of the eruption) the total amount of SO_2 present in atmosphere, estimated by IASI measurements, is generally below 0.2 Tg. During the last part of the eruption (phase III) the values are one order of magnitude higher, with a maximum of 0.14 Tg measured on 9 May with the afternoon orbits.

IASI SO_2 retrieval

E. Carboni et al.

Title Page

Abstract

Introduction

Conclusions

References

Tables

Figures

◀

▶

◀

▶

Back

Close

Full Screen / Esc

Printer-friendly Version

Interactive Discussion



1 Introduction

The magmatic process of an active volcano (during both quiescent and eruptive phase) could be monitored and explained by observation of volcanic emission into atmosphere. Particularly important is the emission of sulphur dioxide (SO_2) as it is, typically the third most abundant gas, after water vapour and CO_2 , emitted by volcanoes (Prata et al., 2009). Improved satellite remote sensing analysis is important because this can allow the monitoring of unrested and dangerous volcanoes that are in remote areas and not monitored by ground data. Moreover often the SO_2 volcanic plume can be used as a proxy for with volcanic ash (Thomas and Prata, 2011), especially within a few hours of release when the effect of wind shear and gravitation have not divided the ash plume from the SO_2 .

In the last 30 yr (Total Ozone Mapping Spectrometer-TOMS, data from 1979) the presence of SO_2 absorption bands in ultraviolet (UV) and infrared (IR) region has allowed satellite observations to monitor explosive volcanic activity (Prata et al., 2003). Satellite retrievals could be a safe source of information in case of volcanic eruptions, but are less sensitive to low amounts of SO_2 (e.g. quiescent degassing) than ground monitoring. In recent years more advanced, high resolution spectrometers, such as Ozone Monitoring Instrument (OMI) on board of AURA from 2004, Infrared Atmospheric Sounding Interferometer (IASI) and Global Ozone Monitoring Experiment-2 (GOME-2) on board of METeorological OPERational satellite program (METOP) from 2006, have made possible the study of quiescent volcanic activity (Carn et al., 2008).

Near-real time estimate of SO_2 are available globally (from OMI, GOME-2, Scanning Imaging Absorption spectrometer for Atmospheric Cartography-SCHIAMACHY, IASI data) for hazard warning purposes. The accuracy of this data is restricted by the assumptions made (e.g. the altitude of the volcanic plume) in order to provide a fast responsive system (near real time). Furthermore this data does not usually provide reliable estimates of the associated error. As shown by Thomas et al. (2009) the total tonnages retrieved by different UV and IR sensors are variable and highly dependent

Title Page

Abstract

Introduction

Conclusions

References

Tables

Figures



Back

Close

Full Screen / Esc

Printer-friendly Version

Interactive Discussion



on the prescribed plume altitude. They can be useful for aviation hazard but are less reliable for scientific studies.

Due to the complementary nature of ground and satellite measurements (ground measurement are usually available in degassing/quiescent phase with less SO₂, satellite measurements are more reliable during explosive phase with a lot of SO₂) at present no satellite retrieval is properly validated. At present only the OMI retrieval team have published a validation paper, but it is limited to one eruption case, with small amounts (less than 3 DU) of SO₂ in UTLS conditions. Validation of larger amounts SO₂ in fresh volcanic eruption clouds and of lower tropospheric SO₂ in quiescent volcanic plumes is needed (Spinei et al., 2010).

Satellite infrared spectrometer can measure volcanic SO₂ on three spectral regions around 4.0, 7.3 and 8.7 μm (called respectively $\nu_1 + \nu_3$, ν_3 and ν_1 absorption band). The 4.0 μm absorption feature ($\nu_1 + \nu_3$) is weak and affected by reflected solar radiation during daytime retrievals. It has been used, for IASI retrievals, when large amounts of SO₂ saturate the signal in the other absorption bands (Karagulian et al., 2010). The 7.3 μm feature (ν_3) is the strongest of the three bands. It is collocated with a strong water vapour absorption band and, as a consequence: (i) it is not very sensitive to surface and lower atmospheric layers; (ii) because water vapour and SO₂ have uncorrelated spectral absorption features, it contains valuable information on SO₂ vertical profile.

The 7.3 μm feature (ν_1 band) has been used in previous optimal estimation retrievals (Clarisse et al., 2008) and in brightness temperature difference alert system by University of Brussels (ULB MeTop/IASI SO₂ Alerts).

The 8.7 μm absorption feature (ν_3 band) contain information on SO₂ amount also for lower tropospheric plumes. This region is an atmospheric window (relatively high transmittance), but by itself does not contain significant spectral information about the plume altitude/profile. Nevertheless it is probably the most useful region for monitoring those volcanoes characterized by continuous quiescent degassing (Merucci, 2011).

In this paper we present a new optimal estimation scheme to retrieve SO₂ from nadir satellite thermal infrared measurements using the ν_3 and ν_1 absorption bands. This

IASI SO₂ retrieval

E. Carboni et al.

Title Page

Abstract

Introduction

Conclusions

References

Tables

Figures

◀

▶

◀

▶

Back

Close

Full Screen / Esc

Printer-friendly Version

Interactive Discussion



retrieval uses a new approach to compute and use the measurement covariance matrix, S_y . Any differences, not related to SO_2 , between IASI spectra and those simulated by a forward model, are included in the covariance matrix allowing a comprehensive error budget to be computed for every pixel. This paper has three main objectives: (1) to describe the algorithm; (2) to assess the performance and data quality of the SO_2 retrieval from IASI measurements; (3) to apply the new retrieval to analyse the volcanic eruption of Eyjafjallajökull during April and May 2010.

2 METOP-IASI data

IASI is on board of METOP, a European meteorological satellite that is operational from 2007. METOP is the first of three satellites that are planned to operate for fourteen years. It crosses the equator on the descending node at a local time of 9.30 a.m. IASI is a Fourier transform spectrometer, that covers the spectral range 645 to 2760 cm^{-1} (3.62–15.5 μm) with a spectral sampling of 0.25 cm^{-1} and a apodised spectral resolution of 0.5 cm^{-1} (Blumstein et al., 2004). It has a nominated radiometric accuracy of 0.25–0.58 K. The IASI field-of-view (FOV) consists of four circular footprints of 20 km diameter (at nadir) inside a square of 50 \times 50 km, step-scanned across track (30 steps). It has a 2000 km wide swath and nominally can achieve global coverage in 12 h (although there are some gaps between orbits near the Equator). Observations are collocated with the Advanced Very High Resolution Radiometer (AVHRR) that provides complementary visible/near infrared measurements. IASI makes nadir observation of the earth simultaneously with Global Ozone Monitoring Experiment (GOME-2) also on board of METOP. GOME-2 is an UV spectrometer that measures SO_2 in the UV absorption band and has been used for both DOAS (Rix et al., 2012) and optimal estimation retrievals (Nowlan et al., 2011) of SO_2 . More information on IASI can be founded in (Clerbaux et al., 2009).

Title Page

Abstract

Introduction

Conclusions

References

Tables

Figures

◀

▶

◀

▶

Back

Close

Full Screen / Esc

Printer-friendly Version

Interactive Discussion



In this work IASI level 1c data (geolocated and apodised spectra), obtained from both the British Atmospheric Data Center (BADc) archive and EUMETSAT Unified Meteorological Archive Facility (UMARF) archive, are used.

3 Fast forward model

To simulate the IASI brightness temperature (BT) we use a radiative transfer code based on RTTOV v.9 (Saunders et al., 1999) available from Met-Office. The fast forward model simulate the IASI signal as function of atmospheric profile (temperature, pressure, SO₂, H₂O, CO₂, CO, O₃, N₂O and CH₄) and surface parameters (temperature and spectral emissivity). RTTOV v.9 does not model variable amounts of SO₂, so here we use a modified version of RTTOV. The SO₂ coefficients are based on regressing existing predictors for CO against transmissions computed using an accurate line by line model, reference forward model (RFM). These calculations are based on the same set of 83 profiles used to train RTTOV for IASI (Matricardi, 2008) to which SO₂ profiles have been added such that the amount varies from 0.1 to 100 DU in several layers from the surface to 21 km altitude. The method is described in more detail in (Siddans, 2011). The SO₂ coefficient are computed in the spectral ranges 1094.75–1232 and 1325–1449.5 cm⁻¹ that includes the two absorption feature around 7.3 and 8.7 μm. The SO₂ feature around 4 μm at present is not included in this fast forward model. RTTOV consider an atmosphere with 90 layers divided by 91 levels, where the first level is the Top Of Atmosphere (TOA). The output given at TOA, at every channels (ch), are radiances ($L(ch)$) and brightness temperatures (BT(ch)).

The forward model provides the weighting functions K_P that represent the derivative of the signal (brightness temperature in (K)) with respect to the variation of the parameters P (e.g., gas amount or surface temperature).

$$K_P(ch) = \frac{\partial BT(ch)}{\partial P} \quad (1)$$

[Title Page](#)[Abstract](#)[Introduction](#)[Conclusions](#)[References](#)[Tables](#)[Figures](#)[◀](#)[▶](#)[◀](#)[▶](#)[Back](#)[Close](#)[Full Screen / Esc](#)[Printer-friendly Version](#)[Interactive Discussion](#)

When the parameter P is a profile $P(\text{layer})$ (as for temperature and gas profiles), K_P will be a function of the channel and the perturbed layer ($K_P(\text{ch}, \text{layer})$)

Figure 1 shows the spectra, obtained for standard atmospheric profiles, of brightness temperature and transmittance together with the weighting function with respect to variation in surface temperature (K_t), followed by the weighting function respect to the gas profiles ($K_P(\text{ch}, \text{layer})$) that affect the spectral region around the SO_2 ν_1 and ν_3 absorption band. The plot of the transmittances (Fig. 1b) shows the channels that will be more influenced by an additional layer of cloud or ash/aerosol as well as by change in surface temperature (as show in Fig. 1c). The plot of the weighting functions with respect the temperature profile shows that the brightness temperature measured in this spectral range is affected by the temperature profile between 0 and 10 km (mainly because of water vapour presence) especially the $\nu > 1200 \text{ cm}^{-1}$. On the left side of the plotted spectra there is the ozone absorption band, this if followed by a relatively transparent part of the spectra (atmospheric window between $1100\text{--}1200 \text{ cm}^{-1}$) that contains some SO_2 and N_2O absorption (not correlated to each other). In the following part of the spectra (from 1200 cm^{-1}) there is strong water vapour absorption together with strong features for N_2O , CH_4 and the relatively strong SO_2 absorption (ν_3). The last part of the spectra is affected by water vapour, SO_2 and CH_4 but these spectral behaviours are not correlated each other.

The atmospheric profiles of temperature, pressure and water vapour are taken from ECMWF data and linearly interpolated to the time of the measurements. Ozone, N_2O and CH_4 are taken as from the standard atmosphere defined in GOMETRAN (Rozanov et al., 1997) and are not varied.

Figure 2 presents the brightness temperature spectra simulated with standard atmosphere and with the addition of a tropospheric (Fig. 2a) and stratospheric (Fig. 2b) SO_2 plume of both: 10 and 100 DU. Using the same spectra, Fig. 2c, d shows the difference between the BT of standard atmosphere and the atmosphere with an SO_2 plume.

Figure 2 show that IASI spectra is sensitive to both the amount of SO_2 and the altitude of the plume. The amount and altitude have different spectral signatures that allow

[Title Page](#)[Abstract](#)[Introduction](#)[Conclusions](#)[References](#)[Tables](#)[Figures](#)[I◀](#)[▶I](#)[◀](#)[▶](#)[Back](#)[Close](#)[Full Screen / Esc](#)[Printer-friendly Version](#)[Interactive Discussion](#)

[Title Page](#)[Abstract](#)[Introduction](#)[Conclusions](#)[References](#)[Tables](#)[Figures](#)[◀](#)[▶](#)[◀](#)[▶](#)[Back](#)[Close](#)[Full Screen / Esc](#)[Printer-friendly Version](#)[Interactive Discussion](#)

the retrieval of both parameters. The spectra of both SO₂ absorption band are attenuated by other atmospheric constituent and considering the same amount of SO₂ we have a higher signal for stratospheric plume; considering the same altitude the signal increase increasing the amount of SO₂. It is possible to note the symmetric ν_1 absorption signal, that don't change significantly in spectral shape between plume at different altitude. This means that this spectral region doesn't contain information on the plume altitude itself. Instead the spectral shape of ν_3 absorption band is strongly modulated by absorption of other gases (as water vapour) and present a different spectral behaviours for tropospheric or for stratospheric plume. This is the part of the spectra that contain the information on the plume altitude. Note that getting the altitude correct is important not just for itself, but also in order to get the correct amount of SO₂, since the signal depends strongly on altitude.

3.1 SO₂ vertical profile

The SO₂ vertical profile is assumed to be a Gaussian distribution in pressure $G(p)$. The Gaussian is defined by three parameters: the mean p_l , the spread σ and the area A .

$$G(p) = \frac{A}{\sqrt{2\pi\sigma^2}} e^{-\frac{(p-p_l)^2}{2\sigma^2}} \quad (2)$$

Motivation for the choice of this vertical profile is that from a previous sensitivity study (Carboni et al., 2009) where was found that there are between two and three degrees of freedom for SO₂ parameters inside the IASI spectra. Moreover a Gaussian shape allows an analytical (fast) computation of the derivatives.

Here the parameters of the Gaussian are included in the retrieved state vector and are: (1) p_l is the pressure (mb) corresponding to the mean of the Gaussian and this will be called altitude of the plume, (2) σ is the spread (mb) of the Gaussian, and (3) A is the column density of SO₂ (that is the integral of the Gaussian) expressed in DU. For the case of a small-intermediate eruption (such as the one analysed in this paper)

the spread is fixed to 100 mb, but it is a parameter that can be usefully included in the retrieval, in case of larger eruptions (for which the number of degree of freedom is larger).

3.2 Ash and cloud layer

The same scheme of the Oxford-RAL Aerosol and Cloud algorithm (ORAC) infrared forward model has been used to include a layer of scattering and absorbing material in the IASI forward model. The atmosphere above and below the layer is considered to be composed by gas as simulated by RTTOV. More details can be find in (Thomas et al., 2009; Poulsen et al., 2012). This layer can be representative of an aerosol layer (ash, desert dust or maritime) or a water cloud layer. Other types of layer can be easily implemented using the appropriate optical properties.

For any defined type of layer we pre-compute the spectral characteristic in look up table (LUT) as emissivity (ϵ_l), reflectance (R_l) and transmittance (T_l) using DISORT and the optical properties (spectral extinction coefficient, single scattering albedo and phase function) from Mie theory. The LUTs are functions of instrument channel, the geometry of observations, the optical depth and effective radius. In the following all the quantities are function of the instrument channel and observation angles.

The RTTOV outputs at TOA are the upwelling radiances ($L_{\text{clean}}^{\uparrow}$) and the corresponding brightness temperatures (BT). The RTTOV output and derived quantities given at any level are (the dependence from the level is here indicated with the suffix l): transmittance above the level, from TOA to the level, (T_{al}), up-welling radiation from the atmosphere above each level (L_{al}^{\uparrow}), the down-welling radiation ($L_{\text{al}}^{\downarrow}$), the up-welling radiation from the atmosphere below each level ($L_{\text{bl}}^{\uparrow(\text{atm})}$), atmospheric transmittance below the level (T_{bl}).

We combine the atmospheric RTTOV output with the aerosol/cloud properties to obtain the radiance (L_{\bullet}^{\uparrow}) of an atmosphere with an aerosol/cloud layer as follows:

$$L_{\bullet}^{\uparrow} = B_l \epsilon_l T_{\text{al}} + L_{\text{al}}^{\downarrow} R_l T_{\text{al}} + L_{\text{al}}^{\uparrow} + L_{\text{bl}}^{\uparrow} T_l T_{\text{al}} \quad (3)$$

Title Page

Abstract

Introduction

Conclusions

References

Tables

Figures

◀

▶

◀

▶

Back

Close

Full Screen / Esc

Printer-friendly Version

Interactive Discussion



where B_l is the Planck radiance at the temperature of the layer, and the up-welling radiance below the layer L_{bl}^\uparrow takes into account both contributions, the atmosphere below the aerosol layer and surface contribution

$$L_{bl}^\uparrow = L_{bl}^{\uparrow(\text{atm})} + B_s \epsilon_s T_{bl} \quad (4)$$

In particular the dependence to the surface temperature (one element of the state vector, see Sect. 4.1) is through the Planck radiance of the surface B_s . The radiance L_{bl}^\uparrow is then converted to BT and used as simulated IASI spectra.

More than one aerosol/cloud layer can be represented by an extended version of this model (Siddans and Poulsen, 2011; Siddans et al., 2010) but it is not used in the present work.

4 Retrieval algorithm

4.1 Optimal estimation

Using an Optimal Estimation (OE) (Rodgers, 2000) scheme we perform a simultaneous retrieval of SO_2 amount and altitude. Briefly the OE retrieval seeks a minimum for a cost function, J . Finding the minimum of J corresponds to finding the state vector \mathbf{x} that maximizes the probability of obtaining the measurement \mathbf{y}

$$J = (\mathbf{y} - F(\mathbf{x}))^T \mathbf{S}_y^{-1} (\mathbf{y} - F(\mathbf{x})) + (\mathbf{x} - \mathbf{x}_a)^T \mathbf{S}_a^{-1} (\mathbf{x} - \mathbf{x}_a) \quad (5)$$

where usually: \mathbf{y} would contain the measurements, usually spectral radiance or BT; \mathbf{S}_y would represent noise on those measurements; \mathbf{x} is the state vector, the vector of parameter do be retrieved. In principle \mathbf{x} would contain all atmospheric and surface parameters that affect these radiances and are imperfectly known. In this case \mathbf{x} would include water vapour and temperature profiles, cloud properties and many other minor species, as well as SO_2 . The simulated measurements $F(\mathbf{x})$ are obtained with the

Title Page

Abstract

Introduction

Conclusions

References

Tables

Figures

◀

▶

◀

▶

Back

Close

Full Screen / Esc

Printer-friendly Version

Interactive Discussion



forward model. The a priori state vector is \mathbf{x}_a and \mathbf{S}_a is the a priori error covariance matrix. \mathbf{x}_a and \mathbf{S}_a represent our a priori knowledge of the state before the measurement is made, and the precision of this knowledge.

However: (1) we are not interested in most of these potential state variables x ; (2) SO_2 is very rarely present in significant amounts in the IASI spectra (except during volcanic eruptions and degassing regions); (3) water vapour and temperatures are well predicted by meteorological data; (4) other gases and atmospheric constituent (like clouds and ash) have features which are spectrally uncorrelated with SO_2 .

So we can greatly simplify the retrieval problem by including the variabilities coming from all these variables in the measurement error covariance matrix. In other words we include all the differences (or errors), between measured IASI spectra and the one simulated by forward model (using ECMWF profiles), in a new “error covariance matrix” \mathbf{S}_e .

In this way \mathbf{S}_e will include: the instrumental errors (IASI noise), the forward model errors (imperfect representation of radiance within RTTOV), and all the errors due to the imperfect knowledge of the parameters that affect the radiance; e.g. the errors due to the non perfect representation of gas absorption (both profile and spectroscopy), and especially errors due to presence of a cloud layer. In the state vector \mathbf{x} we don't consider any of the parameters that are not related to SO_2 (of with the variability is now represented in the new error covariance matrix), and we leave only: SO_2 amount, altitude of the plume, spread, and surface temperature. The simulated measurements $F(\mathbf{x})$ are computed using the corresponding ECMWF data and the state vector. To perform the retrieval we use the standard OE routine that minimizes the cost function J , and in addition we consider a bias \mathbf{b} between the measurements \mathbf{y} and the simulated spectra $F(\mathbf{x})$.

$$J = (\mathbf{y} - F(\mathbf{x}) - \mathbf{b})^T \mathbf{S}_e^{-1} (\mathbf{y} - F(\mathbf{x}) - \mathbf{b}) + (\mathbf{x} - \mathbf{x}_a)^T \mathbf{S}_a^{-1} (\mathbf{x} - \mathbf{x}_a) \quad (6)$$

The minimization routine uses the Levenberg-Marquard numerical iteration method. Moreover, to perform the iteration we use the weighting function matrix \mathbf{K} , that contains

IASI SO_2 retrieval

E. Carboni et al.

Title Page

Abstract

Introduction

Conclusions

References

Tables

Figures

◀

▶

◀

▶

Back

Close

Full Screen / Esc

Printer-friendly Version

Interactive Discussion



the derivative of the spectra (index i) simulated by the forward model respect to each element of the state vector (index j): SO_2 total column amount, plume altitude, plume spread and surface temperature.

For the first 3 elements (the ones that are also a parameter in the SO_2 Gaussian profile $G(\rho)$) of the state vector we have:

$$\mathbf{K}_{i,j} = \frac{\partial F_i[G_j(x)]}{\partial x_j} = F'[G(x)] \times G'(x) \quad (7)$$

These $\mathbf{K}_{i,j}$ are computed analytically starting from the weighting function K_p (Fig. 1).

4.2 Error covariance matrix

The new error covariance matrix \mathbf{S}_e has been estimate by calculating the difference, between IASI measured spectra and the simulated one, for similar atmospheric conditions, but when there is no SO_2 in the atmosphere. This will give an error covariance matrix which allows deviations due to cloud and trace-gases but still enable the SO_2 signature to be detected.

For Eyjafjallajökull eruption it have been considered all the IASI data, in the same geographic region (between 45° and 70° of latitude and between -40° and 10° longitude), of the same month, the year before (eg. April or May 2009). For every pixel we have the IASI measurement y and we compute the simulated one, y_s , with the forward model (where the SO_2 amount is fixed to zero) and the corresponding ECMWF data (e.g. $y_s = F(\mathbf{x}_0 = 0)$). Each element of the covariance matrix has been computed as follows (i and j are indices corresponding to the IASI channels):

$$\mathbf{S}_e(i, j) = \langle (y_i - y_{si}) - \overline{(y_i - y_{si})} \rangle \langle (y_j - y_{sj}) - \overline{(y_j - y_{sj})} \rangle \quad (8)$$

where the term $\overline{y_i - y_{si}}$ is the average spectra of differences between measurements and simulations. This is the bias term (b) that is considered inside the cost function (Eq. 6) during the retrieval.

Title Page

Abstract

Introduction

Conclusions

References

Tables

Figures

◀

▶

◀

▶

Back

Close

Full Screen / Esc

Printer-friendly Version

Interactive Discussion



The error covariance matrix, computed in this way, will include the variability of every atmospheric constituent that are not represented by the forward model (e.g. presence of cloud, error in ECMWF profiles, wrong spectroscopy of minor gases . . .) as well the instrumental error. It will not include any spectral behaviours of SO₂ because it have been deliberately chosen to compute the covariance matrix with IASI pixels that are not affected by any volcanic plume or strong industrial pollution. All the error/variability represented in the covariance matrix will be included in the output error of the retrieved state vector at any pixel as suggested by Von Clarmann et al. (2001).

The error of the retrieved state can be described by the covariance matrix:

$$\hat{\mathbf{S}} = (\mathbf{S}_a^{-1} + \mathbf{K}_i^T \mathbf{S}_e^{-1} \mathbf{K}_i)^{-1} \quad (9)$$

(computed for \mathbf{K}_i evaluated at final iteration i , when convergence has been achieved).

Because (i) the computation of a covariance matrix based on a big ensemble of IASI pixels with the same climatology (as the same month the year before) requires long computation time (longer than the retrieval itself if applied to sporadic volcanic eruption) and (ii) the impossibility of selecting IASI pixels that are not affected by SO₂ in some regions where there is particularly active volcano degassing, a global error covariance matrix has also been computed in the same manner as the “local” one. For the global covariance, we considered all the IASI data of four days (one every season) of 2009 (more than 5 million pixels). This global covariance matrix can be applied globally, but doing so may be expected to lead to higher estimated errors in SO₂ because more variability is included in the \mathbf{S}_e . Both covariance matrices are analysed in the following section.

5 Error analysis

Retrievals are performed on simulated data to assess the sensitivity of the retrieved parameters to perturbations in the state. The performance of the retrieval is evaluated using the information content of the measurements in these idealised circumstances.

Title Page

Abstract

Introduction

Conclusions

References

Tables

Figures

◀

▶

◀

▶

Back

Close

Full Screen / Esc

Printer-friendly Version

Interactive Discussion



Here the linear error of the state vector and results of the retrieval using simulated data are investigated. The retrieval is performed on synthetic spectra produced with values that cover all the realistic range of the parameters we want to retrieve. In this retrieval we use the same \mathbf{S}_e and a priori setting as for the proper retrieval but we don't subtract the bias (between simulation and measurements) in the computation of the cost function. The a priori values used for SO_2 and plume altitude are 0.5 DU and 400 mb with respectively 100 DU and 1000 mb of a priori error. A priori surface temperature is set to the temperature of the first atmospheric layer with 20 K of error.

The linear error in the estimate state is obtained with (Rodgers, 2000):

$$10 \quad \mathbf{S}_x = (\mathbf{K}^T \mathbf{S}_e^{-1} \mathbf{K} + \mathbf{S}_a^{-1})^{-1} \quad (10)$$

where the weighting function \mathbf{K} is computed at the values x . The degrees of freedom are obtained by taking the inverse of Eq. (10):

$$\mathbf{S}_x^{-1} = \mathbf{K}^T \mathbf{S}_y^{-1} \mathbf{K} + \mathbf{S}_a^{-1} \quad (11)$$

which can be reorganised to:

$$15 \quad \mathbf{K}^T \mathbf{S}_y^{-1} \mathbf{K} = \mathbf{S}_x^{-1} - \mathbf{S}_a^{-1} \quad (12)$$

From Rodger (2000) the averaging kernel \mathbf{A} can be written as:

$$\mathbf{A} = \mathbf{S}_x \mathbf{K}^T \mathbf{S}_y^{-1} \mathbf{K} \quad (13)$$

Substituting in Eq. (12) gives:

$$\mathbf{A} = \mathbf{S}_x \mathbf{S}_x^{-1} - \mathbf{S}_a^{-1} \quad (14)$$

20 The sum of the elements of the diagonal (trace) of \mathbf{A} give the degree of freedom (DF) of the retrieval. DF can be interpreted as the number of parameters (of the state vector) that can be independently retrieved.

Title Page

Abstract

Introduction

Conclusions

References

Tables

Figures

◀

▶

◀

▶

Back

Close

Full Screen / Esc

Printer-friendly Version

Interactive Discussion



IASI SO₂ retrieval

E. Carboni et al.

[Title Page](#)[Abstract](#)[Introduction](#)[Conclusions](#)[References](#)[Tables](#)[Figures](#)[◀](#)[▶](#)[◀](#)[▶](#)[Back](#)[Close](#)[Full Screen / Esc](#)[Printer-friendly Version](#)[Interactive Discussion](#)

Simulations have been performed for SO₂ column amount varying between 0.1 and 100 DU and plume altitude between 100 and 1000 mb. The parameter of the state vector corresponding to the spread of the Gaussian profile is fixed at 100 mb. Two surface temperatures values have been considered: in the first case the surface temperature is set equal to the temperature of the first atmospheric layer (this is the worst case for a nadir retrieval in the thermal infrared); in the second case the surface temperature is set to the first atmospheric layer plus 10 K (this tests the cases that have a good thermal contrast between surface and atmosphere). Hence the retrieval is tested for no and some thermal contrast between the first atmospheric layer and the surface. The error covariance matrices considered are; the “local” covariance matrix, that is the one computed for April above the Icelandic plume region, and a “global” covariance matrix. The local error covariance matrix for May gives results that are similar to using the covariance matrix for April so are not reported here. For all the simulations the standard atmosphere profiles (e.g. temperatures, water vapour, ozone, methane . . .) are used. The values, of the state vector x , used to produce the simulations are shown in Fig. 3 together with the linear errors

on the true state and the degree of freedom.

The Fig. 3 show that the error on SO₂ amount strongly depend on the plume altitude and increase when the plume is going close to the surface. From the other side SO₂ error increase when the SO₂ amount increase. There isn't enough information to retrieve the plume altitude for low amount of SO₂ and for plume close to the surface, except for big amount of SO₂ and good thermal contrast between surface and atmosphere. When there isn't enough information the resulting error in altitude is the a priori error. This is confirmed by the degrees of freedom (DF) plots, the area with DF close to two strictly correspond to the area with maximum error in plume altitude. The conditions, that in DF plots present tree DF or more, correspond to the case in which we can retrieve all the tree parameters in the state vector, and correspond to lower error in the plume altitude. The errors behaviours are independent from the error covariance matrix used (global or local).

IASI SO₂ retrieval

E. Carboni et al.

[Title Page](#)[Abstract](#)[Introduction](#)[Conclusions](#)[References](#)[Tables](#)[Figures](#)[◀](#)[▶](#)[◀](#)[▶](#)[Back](#)[Close](#)[Full Screen / Esc](#)[Printer-friendly Version](#)[Interactive Discussion](#)

The minimum error in SO₂ amount is decreasing with the increase of the plume altitude. Assuming a known plume altitude, and converting pressure values into km through the standard atmospheric profile, the values of the minimum error obtained are around two DU for plume centred at 1.5 km and go to 1 DU (and less) for 3 km altitude (and more) arriving to 0.25 DU at 11 km.

Figure 4 shows the results of the retrieval, for the three state vectors parameters (SO₂ amount, altitude and surface temperature), using the synthetic spectra for different conditions as illustrated in Fig. 3, using both local and global error covariance matrix and with or without thermal contrast between surface and atmosphere.

The conditions with thermal contrast produce better retrievals for plume close to the surface. When there isn't not enough information, to retrieve also the plume altitude, the retrieval produces the a priori values of 600 mb and consequently the SO₂ amount for conditions close to the surface are underestimated. Note that retrievals of low amount of SO₂ with plume close to the surface, can produce negative values of SO₂. The equivalent error plots are not shown but the behaviour is similar to Fig. 3.

Moreover the retrievals for true conditions with plume altitude around the tropopause can jump between the altitude values with the same temperature, these produce wrong retrieval values of plume altitude but don't affect significantly the retrieved values of SO₂ amount. In fact the volcanic plume in these conditions is well above the tropospheric boundary layer that contains the majority of water vapour (that is the main cause of extinction in the atmosphere in the ν_3 band) and the SO₂ signal itself is not varying between these same temperature layers. So they are mainly indistinguishable from the retrieval and the altitude results depend strongly on the first guess, but the amount of retrieved SO₂ is nevertheless reliable.

5.1 Influence of ash and cloud layer

To investigate the influence in the SO₂ retrieval due to the presence of an ash or cloud layer, synthetic spectra computed with the forward model with an ash and cloud layer (Sect. 3.2) have been computed and used (as IASI measurements) to perform the re-

trieval without taking into account the layer. Synthetic spectra have been computed for different ash optimal depth (from 0.2 to 2) and effective radius of 2 μm , water cloud optical depth (from 1 to 30) and effective radius of 15 μm . Simulation have been done with different altitudes of the layer between 1000 mb and 200 mb. All the synthetic spectra have been computed with 50 DU of SO_2 and 400 mb of altitude (true state vector) and no thermal contrast between surface and first atmospheric layer (both equal to 270 K).

The results of the retrieval are presented in Fig. 5. The presence of ash with more than one AOD, within the extension of the SO_2 plume (Gaussian vertical profile), can affect significantly the retrieval of SO_2 amount, producing an underestimation of around 50 % of the true amount. These conditions are also producing a cost function higher than two and consequently are discernible, and it is possible to flag them a posteriori. A possible option, for future work, will be to perform both SO_2 and ash retrieval simultaneously in these pixels. The presence of cloud below the SO_2 plume don't affect significantly the retrieval, as expected because the cloud signal is included in the variability considered in the error covariance matrix. As soon as the cloud layer start to overcome some layers with presence of SO_2 (defined by the Gaussian profile with 400 mb altitude and a spread of 100 mb) the cloud smooth the spectral signal of the underling SO_2 and the SO_2 amount is underestimate. The cloud presence can arrive to cover the SO_2 signal completely and to produce retrieval with really low or zero amount of retrieved SO_2 for conditions with a thick cloud over-line the SO_2 plume. Note that these conditions are not distinguishable by the simple cost function criteria, in fact in all these simulation the cost function values arrive at maximum at 1.4 values.

Mainly the error covariance matrix is computed including the spectra variability due to cloudy and non cloudy pixels and, as effect of this, the retrieval is not affected by presence of cloud below the plume. From the other side the presence of cloud in a pixel can not be discernible troughs the cost function values.

The retrieval present in this paper is mainly based on fit the SO_2 spectral shape and spectral variability, due to cloud presence or surface temperature or other spectral behaviours considered in the covariance matrix, are not influencing the resulting SO_2

[Title Page](#)[Abstract](#)[Introduction](#)[Conclusions](#)[References](#)[Tables](#)[Figures](#)[I◀](#)[▶I](#)[◀](#)[▶](#)[Back](#)[Close](#)[Full Screen / Esc](#)[Printer-friendly Version](#)[Interactive Discussion](#)

amount, but if something produce a different SO₂ spectral shape (e.g. cloud that cover the SO₂ spectra) this affect the retrieval. To conclude, the presence of cloud and ash within the plume practically is equivalent to a smoothing of the SO₂ spectral signature and, even if with different amplitude, produce both an underestimation of the total column amount of SO₂ retrieved. This behaviours is the opposite of what happen in SO₂ retrievals that are based only on the SO₂ absorption (compare to fit the SO₂ spectral shape) as the one commonly used for imager (Corradini et al., 2008). In this imager SO₂ retrieval scheme, the presence of ash decrease the radiance measured in the SO₂ channels and, if not corrected, this produce and overestimation of SO₂ when ash is present (Corradini et al., 2010).

6 Case study: Eyjafjallajökull eruption in April and May 2010

Here the SO₂ retrieval is applied to the case study of the Eyjafjallajökull eruption, to follow the volcanic plume during April and May 2010.

The Eyjafjallajökull is a stratovolcano, located close to Iceland's southern coast, at 63°38' N 19°36' W with an elevation of 1666 m. As reported by Global volcanism program (2011), after an initial eruptive phase (from 20 March 2010) of lava flow but no significant ash and SO₂ emission, an explosive eruptive phase of the Eyjafjallajökull volcano began on the 14 April 2010. This was anticipated by a series of earthquakes in the night between 13 and 14 April.

Following Zehner et al. (2010), the explosive part of this eruption can be divided into three phases:

Phase I: 14–18 April

A phreatomagmatic eruption phase, ice and water from the ice cup above the caldera are directly in contact with the fresh magma in the vent. This produce a faster cooling of the ejected magma and large amount of ash injected in the atmosphere, as well as steams plumes. During this period the injection altitude of the plume is estimate

Title Page

Abstract

Introduction

Conclusions

References

Tables

Figures

◀

▶

◀

▶

Back

Close

Full Screen / Esc

Printer-friendly Version

Interactive Discussion



between 2 and 10 km height (Marzano et al., 2011; Stohl et al., 2011) and the wind conditions transport the ash plume in SE direction, toward Europe.

Phase II: 18 April–4 May

From the evening of 18 April there is a magmatic eruption phase; water and ice from the glacier are not inside the vent. The intensity of the eruption is one order of magnitude lower than phase I, and there is a consistent reduction of ash transported in atmosphere. The altitude of the eruption column is between 2 and 5 km (Zehner et al., 2010; Stohl et al., 2011).

Phase III: 5–24 May

Between 3–5 May an increased seismic activity has been reported and it is followed by a more intense explosive phase of the eruption. Ash production increased and the eruption column altitude is reported between 4 and 10 km (Stohl et al., 2011). In this period ash plumes are transported over Europe and Atlantic Ocean.

The volcanic plumes from the eruption of Eyjafjallajökull starting in April 2010 resulted in the cancellation of 107 000 flights over Europe (or 48 % of total air traffic) affecting roughly 10 million passengers. The airline industry lost an estimated 130 million a day during the eight day period when European airspace was closed.

The SO₂ volcanic plume can be tracked from IASI, as presented by (Walker et al., 2011), choosing a statistical criteria for false detection. In this analysis the threshold to define the volcanic plume is fixed to 1 over ten thousand, it means that we are going to have one false detection (a pixel without any volcanic SO₂ detected as volcanic plume) every ten thousand pixels. All the IASI pixels detected as “volcanic plume” are analysed with the SO₂ retrieval.

The first satellite signal from the Eyjafjallajökull eruption is from IASI data on the evening of 14 April (Walker et al., 2012). In the following month we can follow the various phases of the eruption as seen and analysed by various instruments from satellite (Siddans et al., 2011; Francis et al., 2012; Thomas and Prata, 2011; Rix et al., 2012), flights (Rauthe-Schoch et al., 2012; Schumann et al., 2011; Marenco et al., 2011),

IASI SO₂ retrieval

E. Carboni et al.

Title Page

Abstract

Introduction

Conclusions

References

Tables

Figures

◀

▶

◀

▶

Back

Close

Full Screen / Esc

Printer-friendly Version

Interactive Discussion



ground measurements (Mona et al., 2011; Harrison et al., 2010) and dispersion model (Dacre et al., 2011; Stohl et al., 2011).

IASI can follow the SO₂ volcanic plume with an image, composed from multiple orbits, every half day, as show in Figs. 6–8. These plots present the column amount of SO₂ in DU (1 DU = 0.0285 gm⁻²).

The total mass of SO₂ in atmospheric plume is obtained assuming an average area of 25 × 25 km for any IASI pixel and is presented in Fig. 9. The error-bars reported are the worst scenario of correlated error, obtained as sum of all the pixel errors (this overestimates when compared to independent errors). Applying a cut for quality control to the retrieval results, decrease the number of pixels considered in the sum and consequently decrease the total mass of SO₂. Figure 9 show the values of the total mass obtained considering all the plume pixels (with latitude between 30° and 80° N and longitude between -50° and 40° E), and considering only the pixel that pass the quality control criteria (convergence and cost function less than two). The first plume arrives over North Europe on 15 April and it spread over Scandinavia and Central-East Europe over the following three days. This SO₂ plume is “connected” with the volcano location only in the first two images (14 afternoon and 15 morning) and after that it is transported from the meteorological conditions. The fact that there isn’t any SO₂ detectable close to the volcano can be because the volcano itself is no emitting SO₂ or because, in this phreatomagmatic phase, the interaction with water deplete the SO₂ at the source. From morning image of the 18 April, there is a new SO₂ injection in atmosphere. During phase II, magmatic phase (SO₂ is not deplete from the interaction with ice/water in the caldera), the SO₂ plume is identified close to the volcano in nearly all the images between 18 April and 4 May but the amount of SO₂ is one order of magnitude lower compare to the following phase III. Starting from the morning of the 4 May, the SO₂ amount in atmosphere coming from the Icelandic volcano, increase drastically, the total mass of SO₂ is going from 0.01 Tg on 4th morning to 0.14 on 9th afternoon. Between 4 and 8 May the plume overpass the West Europe, in particular UK, Ireland, France and Spain. On 9 May the SO₂ plume is located over the Atlantic ocean (arriving

IASI SO₂ retrieval

E. Carboni et al.

Title Page

Abstract

Introduction

Conclusions

References

Tables

Figures

◀

▶

◀

▶

Back

Close

Full Screen / Esc

Printer-friendly Version

Interactive Discussion



to the coast of Greenland) and on 10th a filament of the plume is overpassing South Europe, starting from Spain and spreading toward east, north-east direction. On 11th morning image a fresh plume is overpassing Ireland and it is blowing into Europe again, at the same time the older and diluted plume is still travelling north-east (crossing all Europe up to Scandinavia on 12 May). Wind condition transport a new SO₂ plume from Icelandic volcano again over Europe on 14 May and 16 and 17 May. The relative minimum of SO₂ amount on 8 May morning on Fig. 9 is due to the missing of one IASI orbit, that presumably contain part of the plume, on the west part of the selected region.

In comparison with SO₂ data from OMI and AIRS (Thomas and Prata, 2011) the SO₂ total mass, retrieved by IASI, have some period where the data are consistent within the IASI error-bars (as phase II) and other where IASI present higher values (as majority of phase III). IASI and OMI have both a maximum on 10 May but the IASI value is nearly double of the OMI one, and relative discrepancy with AIRS is even higher. Taking into consideration that there are some issues related to time differences between Metop and A-train measurements, and looking qualitatively at the OMI SO₂ images of SO₂ plume from Thomas and Prata (2011) and from IAVCEI Remote Sensing Commission (IAVCEI RSC) web page it seem that the disperse plume are often consistent in magnitude with IASI data in the disperse plume and the majority of the difference is in the more fresh part of the plume, more close to the volcano. There are different factors that can affect the SO₂ retrievals in this area as for example the radiative transfer with dense SO₂ and the presence of thick ash within the SO₂ plume. More qualitative comparison between different measurements in thick ash conditions are highly desirable but out of the scope of this paper. Nerveless the fact that IASI values are higher than OMI support the fact that the first source of discrepancies, between IASI, OMI and AIRS instruments, is not the presence of ash is affecting the IASI retrieval, in fact as discussed in the error analysis in case of thick ash IASI retrieval will be underestimated. The IASI SO₂ total amount for the phase II period can be compared also with the GOME-2 SO₂ (Rix et al., 2012) that is on board of the same Metop platform (simultaneous measurements), and results, for 6 to 12 May and for 16 May, in term of total

IASI SO₂ retrieval

E. Carboni et al.

[Title Page](#)[Abstract](#)[Introduction](#)[Conclusions](#)[References](#)[Tables](#)[Figures](#)[◀](#)[▶](#)[◀](#)[▶](#)[Back](#)[Close](#)[Full Screen / Esc](#)[Printer-friendly Version](#)[Interactive Discussion](#)

amount of SO₂, are in good agreement (within the IASI error-bars). For the daytime images of 5 May and from 13 May forward instead the IASI values are lower than the GOME-2 one and, as noticed before, higher than OMI and AIRS values. The IASI SO₂ results, in term of total amount, are between the previous publications of SO₂ datasets for this eruptions, in particular IASI results are higher than OMI for the phase I, comparable with OMI for majority of phase II, and between GOME-2 and OMI results for phase III. It will be interesting to study if the discrepancies could be explained by the differences between plume altitude assumed by the others satellite retrievals and the one retrieved by IASI, or others factor play a key role in producing the discrepancies, but this is leaved for future work on a more comprehensive comparison analysis.

7 Conclusions

A new OE scheme for SO₂ plume have been developed, it retrieve height and amount of SO₂ plume together with the associated pixel-by pixel error estimates. The error covariance matrix is computed using the differences between the measured IASI spectra and the simulated spectra (driven by ECMWF data). This means that all the variability of the IASI signal due to imperfect knowledge of non-SO₂ atmospheric constituents (presence of clouds, differences between the true atmospheric profiles and the ECMWF one, etc. . . .) as well as imperfect radiative transfer simulations (RTTOV approximations, spectroscopic errors, etc. . . .) are included into the retrieval scheme.

The error analysis indicate that: (i) the uncertainty in SO₂ amounts increase for low amount of SO₂, (ii) the minimum error (0.3 DU) is obtained for plume altitude close to the tropopause (where we have the maximum thermal contrast between surface and plume) and it increase going close to the surface.

The forward model include the possibility to simulate an atmosphere with an ash or cloud layer and this feature is used to test that cloud below the plume do not affect the retrieval, as expected because the cloud spectral variability is included in the climatological data used to compute the error covariance matrix. Cloud at the same altitude,

Title Page

Abstract

Introduction

Conclusions

References

Tables

Figures

◀

▶

◀

▶

Back

Close

Full Screen / Esc

Printer-friendly Version

Interactive Discussion



IASI SO₂ retrieval

E. Carboni et al.

[Title Page](#)[Abstract](#)[Introduction](#)[Conclusions](#)[References](#)[Tables](#)[Figures](#)[◀](#)[▶](#)[◀](#)[▶](#)[Back](#)[Close](#)[Full Screen / Esc](#)[Printer-friendly Version](#)[Interactive Discussion](#)

or above the plume, mask the SO₂ signal and produce underestimation of the SO₂ amount. Thick ash can affect the retrieval, with consequent underestimation of the SO₂ amount, this conditions are recognizable from a posteriori quality control (cost function values). A retrieval of the ash parameters (optical depth, altitude and effective radius) is possible within this scheme but because the high variability of ash refractive index, within the thermal infrared spectral range, it is not considered here but future study on this subject, together with the analysis of the SO₂ retrieval performance in presence of a tick ash plume, are desirable.

The results of a medium intensity eruption, as Eyjafjallajökull case study, illustrate that the scheme is able to follow the evolution of the SO₂ plume thought all the eruptive periods and to quantify the SO₂ amount and altitude, including the phase II of the eruption where the intensity of the eruption and the altitude of the plume are lower.

Acknowledgements. E. Carboni, R. Grainger are supported by and contribute to the NERC NCEO Dymanic Earth Geohazard group (COMET+); J. Walker, A. Dudhia, R. Siddans are supported by NERC NCEO Atmospheric Composition group. We aknowledge Pieter Valks for GOME-2 data and Fred Prata for AIRS data and interesting discussions.

References

- Blumstein, D., Chalon, G., Carlier, T., Buil, C., Hébert, P., Maciaszek, T., Ponce, G., Phulpin, T., Tournier, B., Siméoni, D., Astruc, P., Clauss, A., Kayal, G., and Jegou, R.: IASI Instrument: Technical overview and measured performances, Proc. SPIE, 5543, 196–207, 2004.
- Carboni, E. and Grainger, R.: Satellite remote sensing of SO₂ volcanic emission using GOME-2 and IASI data: sensitivity analysis, Geophysical Research Abstract, Vol. 11, Abstract of the contributions of the EGU General Assembly, Vienna, Austria, 20–24 April 2009.
- Carn, S. A., Krueger, A. J., Arellano, S., Krotkov, N. A., and Yang, K.: Daily monitoring of Ecuadorian volcanic degassing from space, J. Volcanol. Geoth. Res., 176, 141–150, 2008.
- Clarisse, L., Coheur, P. F., Prata, A. J., Hurtmans, D., Razavi, A., Phulpin, T., Hadji-Lazaro, J., and Clerbaux, C.: Tracking and quantifying volcanic SO₂ with IASI, the September 2007

IASI SO₂ retrieval

E. Carboni et al.

Title Page

Abstract

Introduction

Conclusions

References

Tables

Figures

◀

▶

◀

▶

Back

Close

Full Screen / Esc

Printer-friendly Version

Interactive Discussion



eruption at Jebel at Tair, *Atmos. Chem. Phys.*, 8, 7723–7734, doi:10.5194/acp-8-7723-2008, 2008.

Clerbaux, C., Boynard, A., Clarisse, L., George, M., Hadji-Lazaro, J., Herbin, H., Hurtmans, D., Pommier, M., Razavi, A., Turquety, S., Wespes, C., and Coheur, P.-F.: Monitoring of atmospheric composition using the thermal infrared IASI/MetOp sounder, *Atmos. Chem. Phys.*, 9, 6041–6054, doi:10.5194/acp-9-6041-2009, 2009.

Corradini, S., Spinetti, C., Carboni, E., Tirelli, C., Buongiorno, M. F., Pugnaghi, S., and Gangale, G.: Mt. Etna tropospheric ash retrieval and sensitivity analysis using moderate resolution imaging spectroradiometer measurements, *J. Appl. Remote Sens.*, 2, 023550, doi:10.1117/1.3046674, 2008.

Corradini, S., Merucci, L., Prata, A. J., and Piscini, A.: Volcanic ash and SO₂ in the 2008 Kasatochi eruption: retrievals comparison from different IR satellite sensors, *J. Geophys. Res.-Atmos.*, 115, D00L21, doi:10.1029/2009JD013634, 2010.

Dacre, H. F., Grant, A. L. M., Hogan, R. J., Belcher, S. E., Thomson, D. J., Devenish, B. J., Marengo, F., Hort, M. C., Haywood, J. M., Ansmann, A., Mattis, I., and Clarisse, L.: Evaluating the structure and magnitude of the ash plume during the initial phase of the 2010 Eyjafjallajökull eruption using lidar observations and NAME simulations, *J. Geophys. Res.*, 116, D00U03, doi:10.1029/2011JD015608, 2011.

Eckhardt, S., Prata, A. J., Seibert, P., Stebel, K., and Stohl, A.: Estimation of the vertical profile of sulfur dioxide injection into the atmosphere by a volcanic eruption using satellite column measurements and inverse transport modeling, *Atmos. Chem. Phys.*, 8, 3881–3897, doi:10.5194/acp-8-3881-2008, 2008.

Francis, P. N., Cooke, M. C., and Saunders, R. W.: Retrieval of physical properties of volcanic ash using Meteosat: a case study from the 2010 Eyjafjallajökull eruption, *J. Geophys. Res.*, 117, D00U09, doi:10.1029/2011JD016788, 2012.

Graf, H. F., Feichter, J., and Langmann, B.: Volcanic sulfur emissions – estimates of source strength and its contribution to the global sulfate distribution, *J. Geophys. Res.*, 102, 10727–10738, 1997.

Global volcanism program: available at: <http://www.volcano.si.edu/world/volcano.cfm?vnum=1702-02=&volpage=weekly>, Smithsonian, last access: December 2011, 2011.

Haywood, J. M., Jones, A., Clarisse, L., Bourassa, A., Barnes, J., Telford, P., Bellouin, N., Boucher, O., Agnew, P., Clerbaux, C., Coheur, P., Degenstein, D., and Braesicke, P.:

IASI SO₂ retrieval

E. Carboni et al.

[Title Page](#)[Abstract](#)[Introduction](#)[Conclusions](#)[References](#)[Tables](#)[Figures](#)[◀](#)[▶](#)[◀](#)[▶](#)[Back](#)[Close](#)[Full Screen / Esc](#)[Printer-friendly Version](#)[Interactive Discussion](#)

Observations of the eruption of the Sarychev volcano and simulations using the HadGEM2 climate model, *J. Geophys. Res.*, 115, D21212, doi:10.1029/2010JD014447, 2010.

Harrison, R. G., Nicoll, K. A., Ulanowski, Z., and Mather, T. A.: Self-charging of the Eyjafjallajökull volcanic ash plume, *Environ. Res. Lett.*, 5, 024004, doi:10.1088/1748-9326/5/2/024004, 2010.

IAVCEI Remote Sensing Commission (IAVCEI RSC): available at: <http://sites.google.com/site/iavenceisweb/eruptions/eyja>, last access: April 2012.

Illingworth, S. M., Remedios, J. J., Boesch, H., Moore, D. P., Sembhi, H., Dudhia, A., and Walker, J. C.: ULIRS, an optimal estimation retrieval scheme for carbon monoxide using IASI spectral radiances: sensitivity analysis, error budget and simulations, *Atmos. Meas. Tech.*, 4, 269–288, doi:10.5194/amt-4-269-2011, 2011.

Karagulian, F., Clarisse, L., Clerbaux, C., Prata, A. J., Hurtmans, D., and Coheur, P. F.: Detection of volcanic SO₂, ash, and H₂SO₄ using the Infrared Atmospheric Sounding Interferometer (IASI), *J. Geophys. Res.*, 115, D00L02, doi:10.1029/2009JD012786, 2010.

Krotkov, N. A., Carn, S. A., Krueger, A. J., Bhartia, P. K., and Yang, K.: Band residual difference algorithm for retrieval of SO₂ from the Aura Ozone Monitoring Instrument (OMI), *IEEE T. Geosci. Remote*, 44, 1259–1266, 2006.

Marenco, F., Johnson, B., Turnbull, K., Newman, S., Haywood, J., Webster, H., and Ricketts, H.: Airborne lidar observations of the 2010 Eyjafjallajökull volcanic ash plume, *J. Geophys. Res.*, 116, D00U05, doi:10.1029/2011JD016396, 2011.

Marzano, F. S., Lamantea, M., Montopoli, M., Di Fabio, S., and Picciotti, E.: The Eyjafjöll explosive volcanic eruption from a microwave weather radar perspective, *Atmos. Chem. Phys.*, 11, 9503–9518, doi:10.5194/acp-11-9503-2011, 2011.

Merucci, L., Burton, M., Corradini, S., and Salerno, G. G.: Reconstruction of SO₂ flux emission chronology from space-based measurements, *J. Volcanol. Geoth. Res.*, 206, 80–87, doi:10.1016/j.jvolgeores.2011.07.002, 2011.

Mona, L., Amodeo, A., D'Amico, G., Giunta, A., Madonna, F., and Pappalardo, G.: Multi-wavelength Raman lidar observations of the Eyjafjallajökull volcanic cloud over Potenza, Southern Italy, *Atmos. Chem. Phys.*, 12, 2229–2244, doi:10.5194/acp-12-2229-2012, 2012.

Nowlan C. R., Liu, X., Chance, K., Cai, Z., Kurosu, T. P., Lee, C., and Martin, R. V.: Retrievals of sulfur dioxide from the Global Ozone Monitoring Experiment 2 (GOME-2) using an optimal estimation approach: algorithm and initial validation, *J. Geophys. Res.*, 116, D18301, doi:10.1029/2011JD015808, 2011.

IASI SO₂ retrieval

E. Carboni et al.

Title Page

Abstract

Introduction

Conclusions

References

Tables

Figures

◀

▶

◀

▶

Back

Close

Full Screen / Esc

Printer-friendly Version

Interactive Discussion



- Prata, A. J.: Satellite detection of hazardous volcanic clouds and the risk to global air traffic, *Nat. Hazards*, 51, 303–324, 2009.
- Prata A. J. and Bernardo, C.: Retrieval of volcanic SO₂ column abundance from atmospheric infrared sounder data, *J. Geophys. Res.*, 112, D20204, doi:10.1029/2006JD007955, 2007.
- 5 Prata, A. J., Rose, W. I., Self, S., and O'Brien, D. M.: Global, long-term sulphur dioxide measurements from TOVS data: A new tool for studying explosive volcanism and climate, in: *Volcanism and the Earth's Atmosphere*, edited by: Robock, A. and Oppenheimer, C., *Geophysical Monograph*, 139, 75–92, 2003.
- Poulsen, C. A., Watts, P. D., Thomas, G. E., Sayer, A. M., Siddans, R., Grainger, R. G.,
10 Lawrence, B. N., Campmany, E., Dean, S. M., and Arnold, C.: Cloud retrievals from satellite data using optimal estimation: evaluation and application to ATSR, *Atmos. Meas. Tech. Discuss.*, 4, 2389–2431, doi:10.5194/amtd-4-2389-2011, 2011.
- Rauthe-Schöch, A., Weigelt, A., Hermann, M., Martinsson, B. G., Baker, A. K., Heue, K.-P., Brenninkmeijer, C. A. M., Zahn, A., Scharffe, D., Eckhardt, S., Stohl, A., and
15 van Velthoven, P. F. J.: CARIBIC aircraft measurements of Eyjafjallajökull volcanic clouds in April/May 2010, *Atmos. Chem. Phys.*, 12, 879–902, doi:10.5194/acp-12-879-2012, 2012.
- Reference forward model – RFM, available at: <http://www.atm.ox.ac.uk/RFM/>, last access: April 2012.
- Rix, M., Valks, P., Hao, N., Loyola, D. G., Schlager, H., Huntrieser, H. H., Flemming, J., Koehler, U., Schumann, U., and Inness, A.: Volcanic SO₂, BrO and plume height estimations using
20 GOME-2 satellite measurements during the eruption of Eyjafjallajökull in May 2010, *J. Geophys. Res.*, 117, D00U19, doi:10.1029/2011JD016718, 2012
- Rodgers, C. D.: *Inverse Methods for Atmospheric Sounding*, World Scientific Series on Atmospheric, Oceanic and Planetary Physics, vol. 2, 2000.
- 25 Rozanov, V., Diebel, D., Spurr, R. J. D., and Burrows, J. P.: GOMETRAN: a radiative transfer model for the satellite project GOME – the plane parallel version, *J. Geophys. Res.*, 102, 16683–16696, 1997.
- Schumann, U., Weinzierl, B., Reitebuch, O., Schlager, H., Minikin, A., Forster, C., Baumann, R., Sailer, T., Graf, K., Mannstein, H., Voigt, C., Rahm, S., Simmet, R., Scheibe, M., Lichtenstern, M., Stock, P., Rüba, H., Schäuble, D., Tafferner, A., Rautenhaus, M., Gerz, T., Ziereis, H.,
30 Krautstrunk, M., Mallaun, C., Gayet, J.-F., Lieke, K., Kandler, K., Ebert, M., Weinbruch, S., Stohl, A., Gasteiger, J., Groß, S., Freudenthaler, V., Wiegner, M., Ansmann, A., Tesche, M., Olafsson, H., and Sturm, K.: Airborne observations of the Eyjafjalla volcano ash cloud over

IASI SO₂ retrieval

E. Carboni et al.

Title Page

Abstract

Introduction

Conclusions

References

Tables

Figures



Back

Close

Full Screen / Esc

Printer-friendly Version

Interactive Discussion



Europe during air space closure in April and May 2010, *Atmos. Chem. Phys.*, 11, 2245–2279, doi:10.5194/acp-11-2245-2011, 2011.

Saunders, R. W., Matricardi, M., and Brunel, P.: An improved fast radiative transfer model for assimilation of satellite radiance observations, *Q. J. Roy. Meteor. Soc.*, 125, 1407–1425, 1999.

Siddans R. and Poulsen C.: EUMETSAT RFQ 10/202688 Towards Detection and Retrieval of Volcanic Ash from SEVIRI using the OCA Processor, 2011.

Siddans, R., Poulsen, C., and Carboni, E.: Cloud model for operational retrievals from MSG SEVIRI, Technical report, European Organisation for the Exploitation of Meteorological Satellites, 2010.

Spinei, E., Carn, S. A., Krotkov, N. A., Mount, G. H., Yang, K., and Krueger, A.: Validation of ozone monitoring instrument SO₂ measurements in the Okmok volcanic cloud over Pullman, WA, July 2008, *J. Geophys. Res.*, 115, D00L08, doi:10.1029/2009JD013492, 2010.

Stohl, A., Prata, A. J., Eckhardt, S., Clarisse, L., Durant, A., Henne, S., Kristiansen, N. I., Minikin, A., Schumann, U., Seibert, P., Stebel, K., Thomas, H. E., Thorsteinsson, T., Tørseth, K., and Weinzierl, B.: Determination of time- and height-resolved volcanic ash emissions and their use for quantitative ash dispersion modeling: the 2010 Eyjafjallajökull eruption, *Atmos. Chem. Phys.*, 11, 4333–4351, doi:10.5194/acp-11-4333-2011, 2011.

Thomas, G. E., Carboni, E., Sayer, A. M., Poulsen, C. A., Siddans, R., and Grainger, R. G.: Oxford-RAL Aerosol and Cloud (ORAC): aerosol retrievals from satellite radiometers, in: *Aerosol Remote Sensing Over Land*, edited by: Kokhanovsky, A. A. and de Leeuw, G., Springer, Berlin, 2009.

Thomas, H. E. and Prata, A. J.: Sulphur dioxide as a volcanic ash proxy during the April–May 2010 eruption of Eyjafjallajökull Volcano, Iceland, *Atmos. Chem. Phys.*, 11, 6871–6880, doi:10.5194/acp-11-6871-2011, 2011. 11863

Thomas, H. E., Watson, I. M., Kearney, C., Carn, S. A., and Murray, S. J.: A multi-sensor comparison of sulphur dioxide emissions from the 2005 eruption of Sierra Negra volcano, Galapagos Islands, *Remote Sens. Environ.*, 113, 1331–1342, 2009.

University of Brussels: ULB MeTop/IASI SO₂ Alerts, available at: <http://cpm-ws4.ulb.ac.be/Alerts/index.php>, last access: April 2012.

Von Clarmann, T., Grabowski, U., and Kiefer, M.: On the role of non-random errors in inverse problems in radiative transfer and other applications, *J. Quant. Spectrosc. Ra.*, 71, 39–46, 2001.

IASI SO₂ retrieval

E. Carboni et al.

[Title Page](#)[Abstract](#)[Introduction](#)[Conclusions](#)[References](#)[Tables](#)[Figures](#)[◀](#)[▶](#)[◀](#)[▶](#)[Back](#)[Close](#)[Full Screen / Esc](#)[Printer-friendly Version](#)[Interactive Discussion](#)

- Walker, J. C., Dudhia, A., and Carboni, E.: An effective method for the detection of trace species demonstrated using the MetOp Infrared Atmospheric Sounding Interferometer, *Atmos. Meas. Tech.*, 4, 1567–1580, doi:10.5194/amt-4-1567-2011, 2011.
- 5 Walker, J. C., Carboni, E., Dudhia, A., and Grainger, R. G.: Improved detection of sulphur dioxide in volcanic plumes using satellite-based hyperspectral infra-red measurements: application to the Eyjafjallajökull 2010 eruption, *J. Geophys. Res.*, 117, D00U16, doi:10.1029/2011JD016810, 2012.
- 10 Watson, I. M., Realmuto, V. J., Rose, W. I., Prata, A. J., Bluth, G. J. S., Gu, Y., Bader, C. E., and Yu, T.: Thermal infrared remote sensing of volcanic emissions using the moderate resolution imaging spectroradiometer, *J. Volcanol. Geoth. Res.*, 135, 75–89, 2004.
- Yang, K., Liu, X., Bhartia, P. K., Krotkov, N. A., Carn, S. A., Hughes, E. J., Krueger, A. J., Spurr, R. J. D., and Trahan, S. G.: Direct retrieval of sulfur dioxide amount and altitude from spaceborne hyperspectral UV measurements: theory and application, *J. Geophys. Res.*, 115, D00L09, doi:10.1029/2010JD013982, 2010.
- 15 Zehner, C. (ed.): Monitoring volcanic ash from space, in: Proceedings of the ESA-EUMETSAT workshop on the 14 April to 23 May 2010 eruption at the Eyjafjöll volcano, South Iceland, Frascati, Italy, 26–27 May 2010, ESA-Publication STM-280, doi:10.5270/atmch-10-01, 2010.

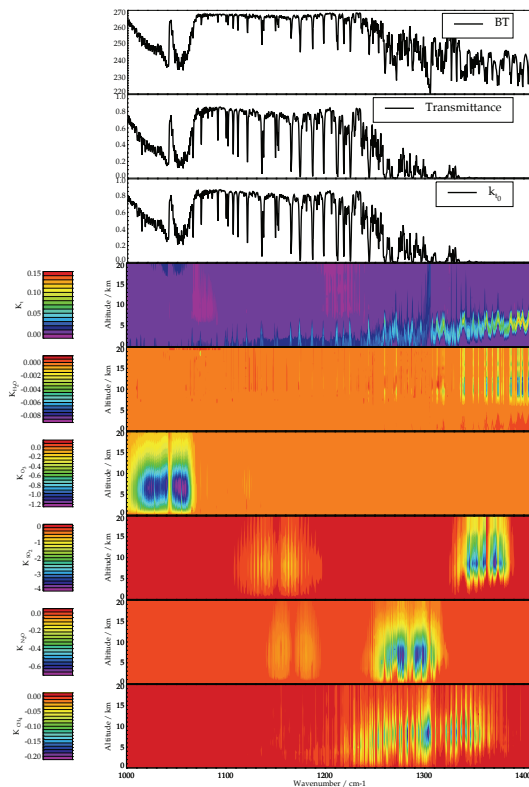


Fig. 1. Spectra obtained for a standard atmosphere profiles of: **(a)** brightness temperature, **(b)** transmittance, **(c)** waiting function with respect to the surface temperature, **(d)** waiting functions with respect to temperature profile (K_T), water vapour profile ($K_{\text{H}_2\text{O}}$), ozone (K_{O_3}), sulphur dioxide (K_{SO_2}), nitrogen dioxide (K_{NO_2}), methane (K_{CH_4}).

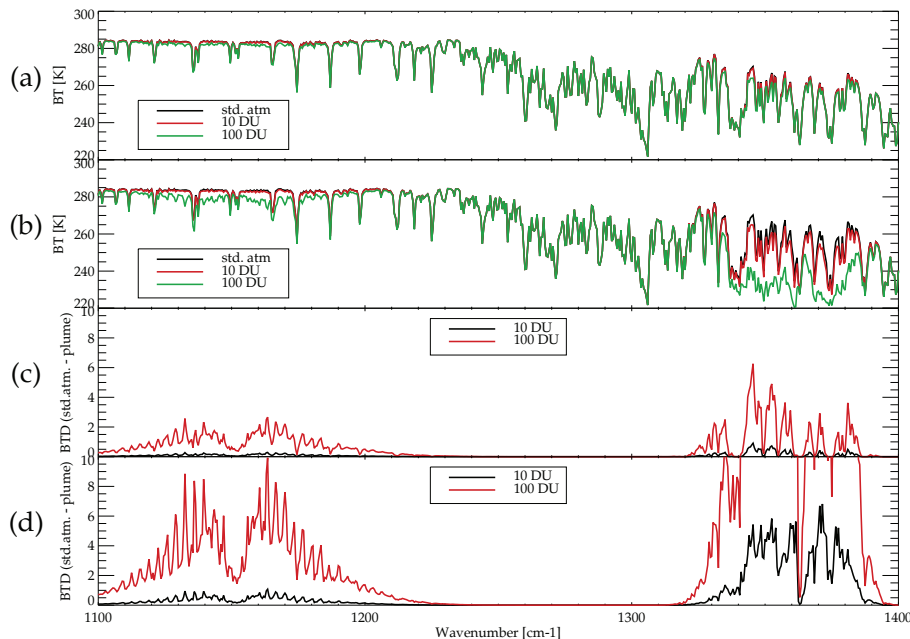


Fig. 2. Simulated IASI spectra: **(a)** brightness temperature (BT) IASI spectra obtained for standard atmosphere (black line) and for standard atmosphere with the addition of a tropospheric SO₂ plume between 1 and 5 km (red line represent a plume of 10 DU, green line a plume of 100 DU); **(b)** the same spectra of standard atmosphere (black line) with the addition of stratospheric volcanic plume between 9 and 14 km (red line represent a plume of 10 DU, green line a plume of 100 DU); simulated brightness temperature differences (BTD) between the standard atmosphere spectra and the one with the volcanic plume plume for: **(c)** tropospheric plume (black line represent a plume with 10 DU of SO₂, red line with 100 DU); **(d)** stratospheric plume (black line represent a plume with 10 DU of SO₂, red line with 100 DU).

[Title Page](#)
[Abstract](#)
[Introduction](#)
[Conclusions](#)
[References](#)
[Tables](#)
[Figures](#)
[◀](#)
[▶](#)
[◀](#)
[▶](#)
[Back](#)
[Close](#)
[Full Screen / Esc](#)
[Printer-friendly Version](#)
[Interactive Discussion](#)

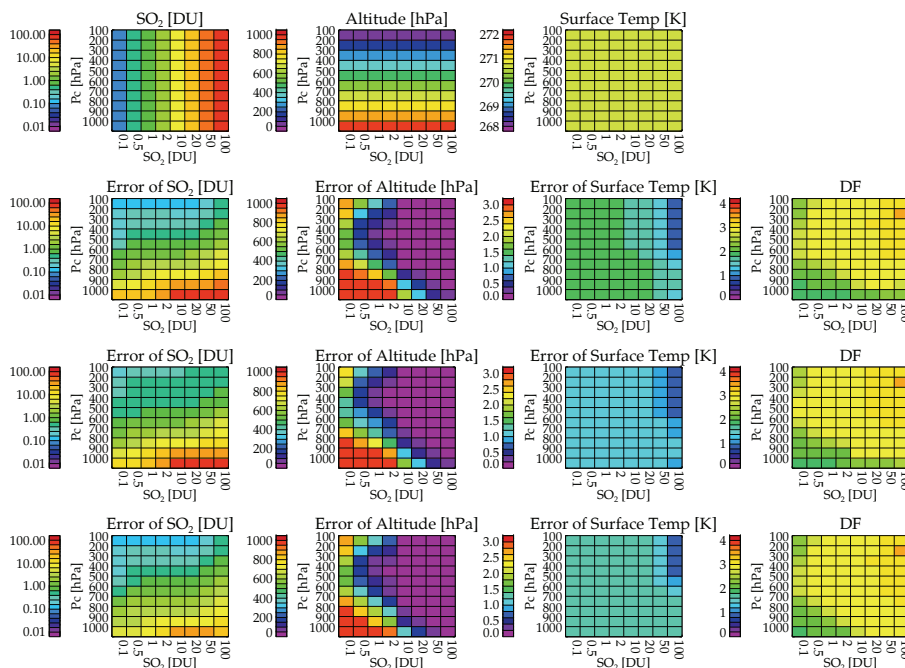



Fig. 3. Values of the state vector used in the simulations together with the linear errors on the state and the degree of freedom. Every plot is a function of SO₂ amount on the abscissae and altitude of the plume on the ordinate. The first line shows the valued of the state vector. The other lines present the corresponding values of the linear error (firsts tree columns) for SO₂ (in logarithmic colour scale), altitude, surface temperature and the degree of freedom (fourth column). Second line present the values obtained using the local error covariance matrix for April and no thermal contrast between surface and atmosphere. Third line is obtained with the global error covariance matrix and no thermal contrast. Last line is obtained with the local covariance matrix and 10 K of thermal contrast between surface and atmosphere.

[Title Page](#)
[Abstract](#)
[Introduction](#)
[Conclusions](#)
[References](#)
[Tables](#)
[Figures](#)
[◀](#)
[▶](#)
[◀](#)
[▶](#)
[Back](#)
[Close](#)
[Full Screen / Esc](#)
[Printer-friendly Version](#)
[Interactive Discussion](#)

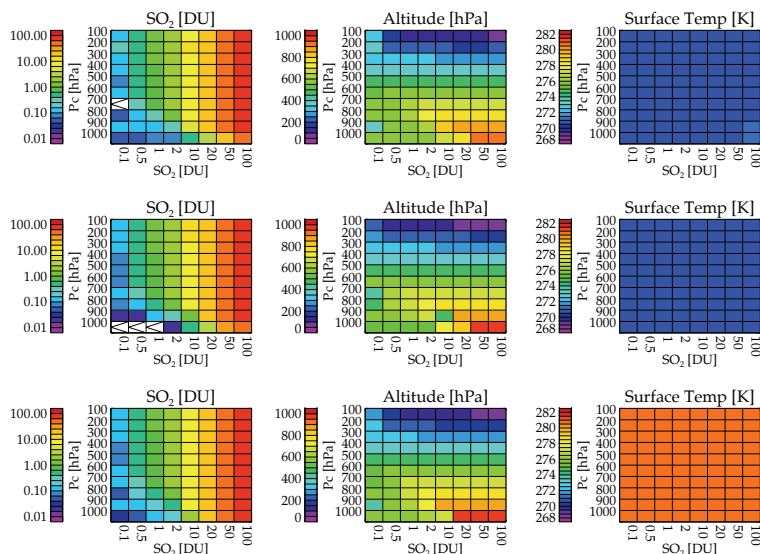
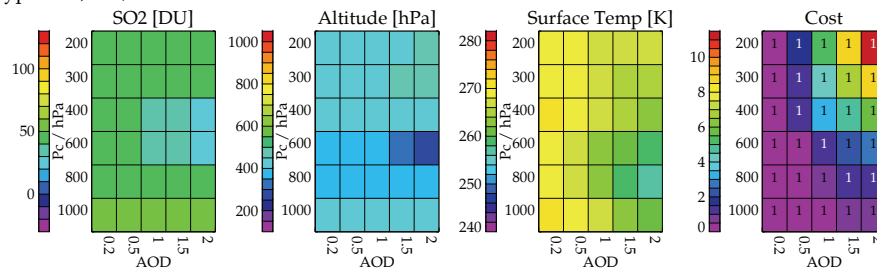



Fig. 4. Retrieved values of the state vector (SO₂ amount, altitude and surface temperature) as a function of SO₂ amount and altitude used in the simulations (“true values”). First line presents the values obtained performing the retrieval with the local error covariance matrix for April and no thermal contrast between surface and atmosphere. Second line presents the values using the global covariance matrix and no thermal contrast. Third line is obtained with the local covariance matrix and 10K of thermal contrast between surface and atmosphere. White box correspond to values below the limit of the colorscale.

[Title Page](#)
[Abstract](#)
[Introduction](#)
[Conclusions](#)
[References](#)
[Tables](#)
[Figures](#)
[◀](#)
[▶](#)
[◀](#)
[▶](#)
[Back](#)
[Close](#)
[Full Screen / Esc](#)
[Printer-friendly Version](#)
[Interactive Discussion](#)


Type: ash, Re / microns = 2



Type: wat, Re / microns = 20

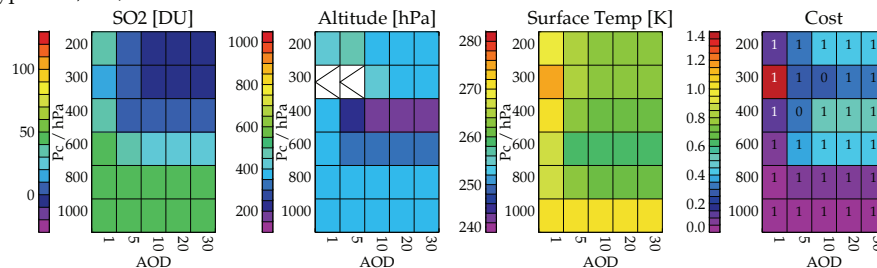


Fig. 5. Values of (first column) SO₂ column amount, (second column) altitude, (third column) surface temperature and cost function obtained from the retrieval using synthetic IASI data with: 50 DU of SO₂ amount, a Gaussian profile centred at 400 mb, 270 K of surface temperature and the presence of an ash or cloud layer. The plots in the first row are with the presence of ash, second with cloud. All the plots are a function of optical depth (in x-axes) and altitude of the layer (y-axes).

Title Page

Abstract

Introduction

Conclusions

References

Tables

Figures

◀

▶

◀

▶

Back

Close

Full Screen / Esc

Printer-friendly Version

Interactive Discussion



IASI SO₂ retrieval

E. Carboni et al.

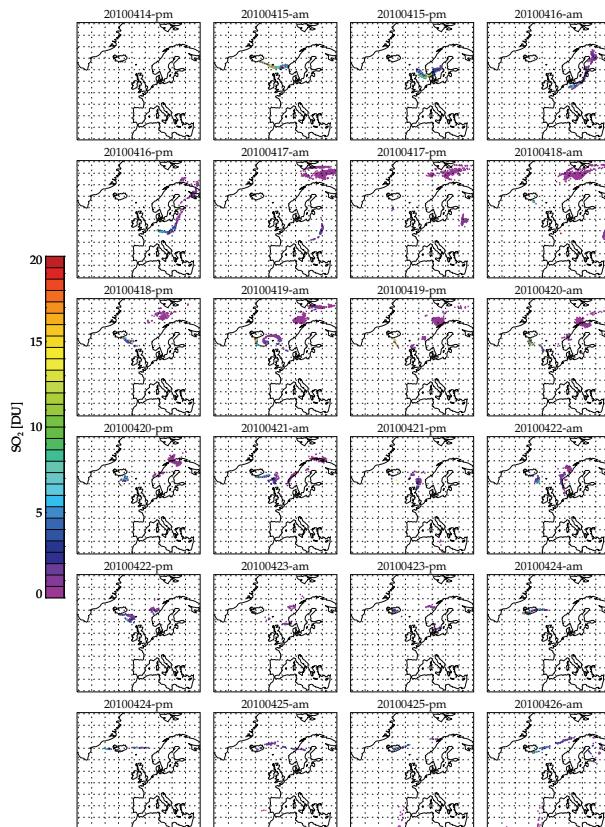


Fig. 6. IASI SO₂ column amount, divided in morning and afternoon orbits, for the period from 14 to 26 April 2010.

[Title Page](#)[Abstract](#)[Introduction](#)[Conclusions](#)[References](#)[Tables](#)[Figures](#)[◀](#)[▶](#)[◀](#)[▶](#)[Back](#)[Close](#)[Full Screen / Esc](#)[Printer-friendly Version](#)[Interactive Discussion](#)

IASI SO₂ retrieval

E. Carboni et al.

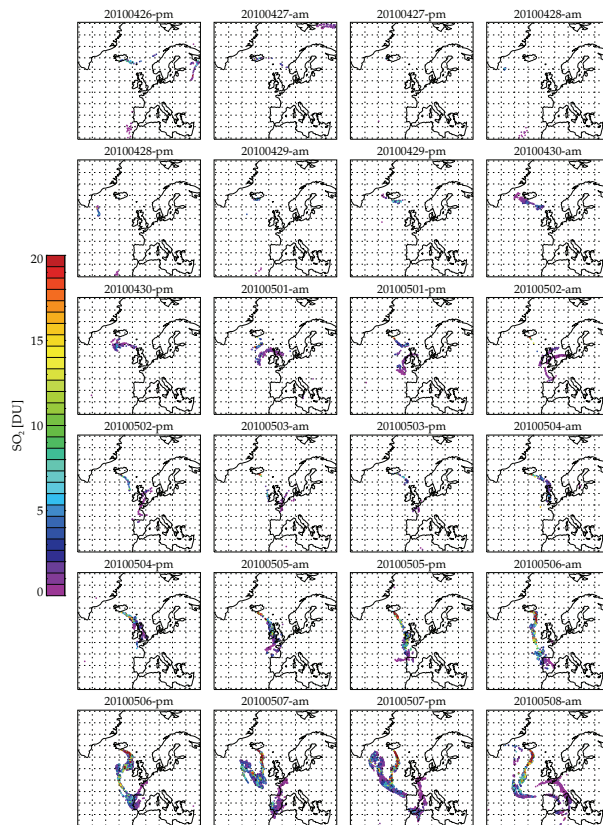


Fig. 7. IASI SO₂ column amount, divided in morning and afternoon orbits, for the period from 26 April 2010 to 8 May 2010.

[Title Page](#)[Abstract](#)[Introduction](#)[Conclusions](#)[References](#)[Tables](#)[Figures](#)[◀](#)[▶](#)[◀](#)[▶](#)[Back](#)[Close](#)[Full Screen / Esc](#)[Printer-friendly Version](#)[Interactive Discussion](#)

IASI SO₂ retrieval

E. Carboni et al.

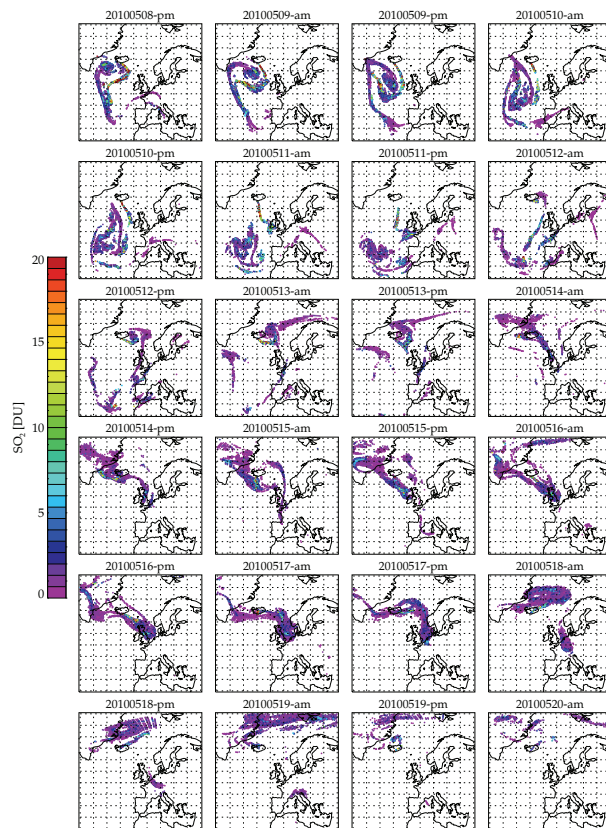


Fig. 8. IASI SO₂ column amount, divided in morning and afternoon orbits, for the period from 8 to 17 May 2010.

[Title Page](#)[Abstract](#)[Introduction](#)[Conclusions](#)[References](#)[Tables](#)[Figures](#)[◀](#)[▶](#)[◀](#)[▶](#)[Back](#)[Close](#)[Full Screen / Esc](#)[Printer-friendly Version](#)[Interactive Discussion](#)

IASI SO₂ retrieval

E. Carboni et al.

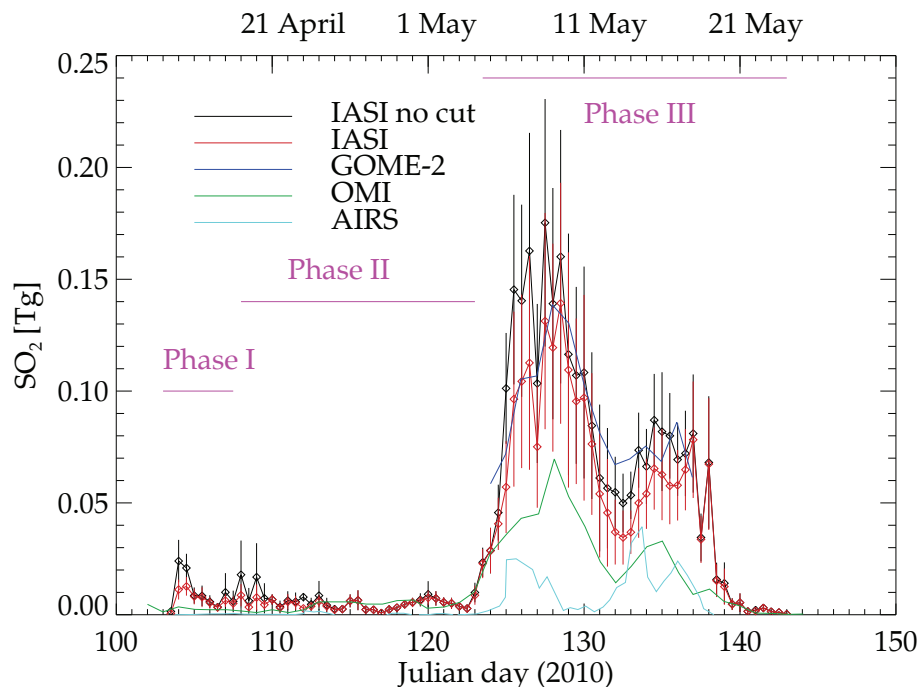


Fig. 9. Estimate of total mass of SO₂ presents in Eyjafjallajökull plume: black line and errorbars are IASI data considering every pixels; red line and errorbars are IASI data using only the pixels that pass the quality control; blu are GOME-2 values from Rix et al. (2012); green are OMI values from Thomas and Prata (2011); cyan are AIRS values from Thomas and Prata (2011).

[Title Page](#)
[Abstract](#)
[Introduction](#)
[Conclusions](#)
[References](#)
[Tables](#)
[Figures](#)
[◀](#)
[▶](#)
[◀](#)
[▶](#)
[Back](#)
[Close](#)
[Full Screen / Esc](#)
[Printer-friendly Version](#)
[Interactive Discussion](#)
